

Photoelectrochemical and XPS characterisation of oxide layers on 316L stainless steel grown in high-temperature water

M. Santamaria¹ · F. Di Franco¹ · F. Di Quarto¹ · M. Pisarek^{2,3} · S. Zanna² · P. Marcus²

Received: 23 January 2015 / Revised: 1 April 2015 / Accepted: 3 April 2015 / Published online: 19 April 2015
© Springer-Verlag Berlin Heidelberg 2015

Abstract Passive films on AISI 316L stainless steel were grown by exposure in high temperature (300 °C and 150 bar) water. X-ray photoelectron spectroscopy was employed to study their composition as a function of immersion time. A photoelectrochemical investigation, supported by electrochemical and impedance measurements, allowed to get information on the solid-state properties of the investigated layers. The experimental results suggest the formation of a stratified layer with an outer iron-rich layer and an inner Cr-rich oxide layer, whose relative thickness and composition are dependent on the immersion time.

Keywords Stainless steel · XPS · Photocurrent spectroscopy · Pressurised water reactor

Introduction

One of the major materials challenge for continued safe, reliable and cost-effective utilisation of water-cooled nuclear reactors for electricity production is the development of improved understanding of the synergistic fundamental mechanisms responsible for corrosion and stress corrosion cracking

degradation of austenitic steels and nickel base alloys [1]. A key factor in determining the corrosion resistance of the materials is played by the properties of the passive films grown on the employed stainless steel during operating conditions. This explains the large interest that, during the years, has been devoted to the structural, morphological and physicochemical characterisation of the passive films grown on such alloys in high-temperature water [2–15]. A survey of the already published works shows that the passive films have a multilayered structure and that the thickness of the film as well as the compositional profile depend on the passivation conditions, i.e., immersion time and water temperature. In spite the large number of published papers, just a few investigations try to study the electronic properties of the passive films, which are expected to play a crucial role in the corrosion resistance of the SS [2, 14].

In the last decades, photoelectrochemical techniques have been employed increasingly for investigating thin photoconducting surface films and corrosion layers on metals and alloys. The advantages are the simplicity of the experimental setup, the insensitivity to surface roughness and the ability to scrutinise very thin films. Moreover, direct information is derived on the electronic properties of the surface films, which are decisive for understanding the corrosion behaviour of metals and alloys [16].

In this work, we studied the solid-state properties of passive layers grown on 316L stainless steel in high-temperature water, under conditions representative of pressurised water reactor (PWR) primary water (300 °C and $P=150$ bar) for different immersion times (from 2 min to 100 h).

A photoelectrochemical investigation was performed in order to estimate the band gap, E_g , of the oxide layers as a function of the immersion time. The dependence of E_g on the immersion time has been rationalised considering changes of the passive layer composition, which has been studied by

✉ M. Santamaria
monica.santamaria@unipa.it

¹ Electrochemical Materials Science Laboratory, DICAM, University of Palermo, Viale delle Scienze, 90128 Palermo, Italy

² Chimie ParisTech-CNRS, Institut de Recherche de Chimie Paris, Research Group Physical Chemistry of Surfaces, PSL Research University, 11 rue Pierre et Marie Curie, 75005 Paris, France

³ Institute of Physical Chemistry, Polish Academy of Science, Warsaw, Poland

X-ray photoelectron spectroscopy (XPS). Impedance measurements were also performed in order to get information on the electronic properties of the alloy/passive film/electrolyte interface with particular interest in the conductivity type of the investigated layers.

Experimental

Electropolished 316L stainless steel samples (17.6 wt% Cr, 12 wt% Ni, 2.39 wt% Mo, 1.78 wt% Mn, 0.59 wt% Si, 0.08 wt% N, 0.028 wt% C and Fe) were exposed to high temperature (300 °C) water at $P=150$ bar for different immersion times (from 2 min to 100 h).

XPS analysis was carried out using a Thermo Electron Escalab 250 spectrometer with a monochromated Al $K\alpha$ radiation (1486.6 eV). The analyser pass energy was 100 eV for survey spectra and 20 eV for high-resolution spectra. The analysed area was 500 μm^2 . The following core levels were analysed: Fe 2p, Cr 2p, Ni 2p, Mo 3d, O 1s and C 1s. The photoelectron take-off angle, between the surface and the direction in which the photoelectrons are analysed, was 90°.

Curve fitting of XPS spectra was performed with the Thermo Electron software Avantage. For the calculation of the surface composition, the inelastic mean free paths calculated by Tanuma et al. [17] and the photoemission cross-sections determined by Scofield [18] were used. A Shirley background was used.

The electrochemical and impedance measurements were performed in 0.25 M Na_2HPO_4 aqueous solution (pH~8.5). The high conductivity of this electrolyte allows to minimise the diffuse double layer contribution to equivalent capacitance.

Photoelectrochemical investigation was carried out in 0.1 M $(\text{NH}_4)_2\text{B}_4\text{O}_7$ (ABE) aqueous solution (pH~8.5) and in 10^{-3} M FeSO_4 aqueous solution (pH~5.5).

The experimental setup for the photoelectrochemical measurements has been described elsewhere [16, 19, 20]. A 450-W UV–vis xenon lamp, coupled with a monochromator, allows irradiation of the specimen through a quartz window. A two-phase, lock-in amplifier, with a mechanical chopper, enables separation of the photocurrent from the total current in the cell. The photocurrent spectra are corrected for the relative photon efficiency of the light source at each wavelength.

Electrochemical impedance spectroscopy (EIS) data were obtained using a Parstat 2263 (PAR), controlled by a computer via Electrochemistry PowerSuite software. A three-electrode arrangement was used, consisting of the specimen, a reference electrode (silver/silver chloride) and a Pt net having a very high specific area, immersed in 0.25 M Na_2HPO_4 (pH~8.5). The impedance spectra were generated by applying a sinusoidal signal of amplitude 10 mV over the frequency range of

0.1 Hz–100 kHz. The recorded spectra were analysed with Zview software.

A silver/silver chloride electrode was employed as a reference for all electrochemical and photoelectrochemical experiments.

Results and discussion

XPS analysis

XPS experiments were carried out after 10 min, 1 h, 5 h, 25 h and 100 h exposure time. The thickness of oxide layers was measured by TOF-SIMS depth profiling on two samples (10 min and 25 h). The measured values are 12 and 16 nm, respectively. Fe 2p_{3/2}, Cr 2p_{3/2} and Ni 2p_{3/2} core level spectra are discussed here. For all exposure times, no metallic species are detected in the spectra, meaning that the oxide layers are thicker than ~10 nm in all cases. XPS analyses are so mainly associated to the outer part of the oxide layers. A weak signal of Mo 3d was detected, but it is not discussed here. Figure 1 shows Cr 2p_{3/2}, Fe 2p_{3/2} and Ni 2p_{3/2} core level spectra after 1 h of exposure time. The Cr 2p_{3/2} core level spectrum exhibits a peak at 577.4 eV associated to Cr^{3+} [21–23]. The Fe 2p_{3/2} core level spectrum presents three peaks at 709.8, 711.3 and 713.1 eV associated to Fe in the 2⁺, 3⁺ oxidation states, and satellite peak, respectively [24–28]. The Ni 2p_{3/2} core level spectrum shows a peak at 856.1 eV associated to Ni^{2+} [29, 30]. A satellite peak is present at 862.4 eV. It may be associated to the presence of $\text{Ni}(\text{OH})_2$ and/or Cr, Fe and Ni spinel species. The intensity ratio between the principal peak and the satellite peak is linked to the chemical environment of Ni^{2+} : The values are 0.28 for $\text{Ni}(\text{OH})_2$, between 0.5 and 0.74 for NiCr_2O_4 and 0.69 for $(\text{Ni}_{0.5}\text{Fe}_{0.5})\text{Cr}_2\text{O}_4$ [14]. The intensity ratio between the Ni 2p_{3/2} principal peak and the satellite peak is between 0.3 and 0.7 in our study and thus is associated to $\text{Ni}(\text{OH})_2$ and/or spinel species like NiCr_2O_4 , $(\text{Ni}_{1-x}\text{Fe}_x^{2+})\text{Cr}_2^{3+}\text{O}_4$ or possibly $(\text{Ni}_{1-y}\text{Fe}_y^{2+})(\text{Fe}_{1-x}\text{Cr}_x^{3+})_2\text{O}_4$. The spectra obtained for the various oxidation times (10 min, 5 h, 25 h and 100 h) are similar to the spectra described above. The same oxidation states have been observed; only the atomic percentage are different. Table 1 gives the chemical composition of the external part of the passive layer. For the short exposure times of 10 min, 1 h and 5 h, enrichment in Ni^{2+} and depletion in Cr^{3+} is observed when the exposure time increases. For the longer exposure, times enrichment of Cr^{3+} is observed.

Figure 2 presents the Fe 2p_{3/2} core level spectra after 1 and 100 h exposure times. The intensity after 100 h is lower than that after 1 h, showing decreasing iron oxide content in the outer part of the passive film for longer exposure times. Moreover the $\text{Fe}^{2+}/\text{Fe}^{3+}$ ratio is higher after 100 h as compared to 1 h exposure time. For long exposure times (25 and 100 h),

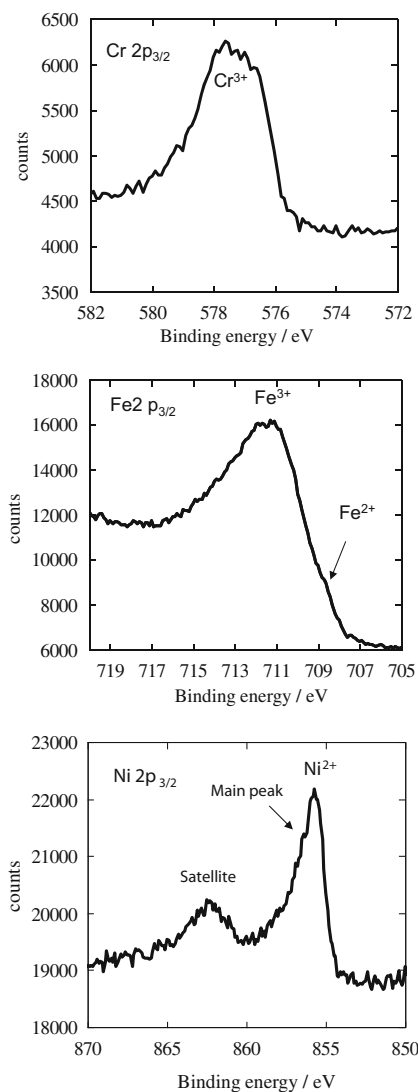


Fig. 1 Cr 2p_{3/2}, Fe 2p_{3/2} and Ni 2p_{3/2} core level spectra after 1 h exposure time to high-temperature water

oxidised iron depletion is observed (see Table 1) as well as enrichment in oxidised chromium. The Fe²⁺/Fe³⁺ depletion and Cr³⁺ enrichment clearly increases from 25 to 100 h of exposure time. The Fe²⁺/Fe³⁺ ratio is higher for longer exposure times (0.64 and 0.82 for 25 and 100 h, respectively) showing Fe³⁺ depletion and Cr³⁺ enrichment for long

Table 1 Atomic composition of the outer passive layer and Fe²⁺/Fe³⁺ atomic ratio as a function of exposure time to high-temperature water

Atomic percent	Fe ³⁺	Fe ²⁺	Cr ³⁺	Ni ²⁺	Fe ²⁺ /Fe ³⁺
10 min	49	13.4	16.9	20.6	0.27
1 h	45.7	18.3	14.7	21.3	0.40
5 h	47	15.9	7.9	29.2	0.34
25 h	32.7	21.1	23.6	22.6	0.64
100 h	17.8	14.6	42.2	25.3	0.82

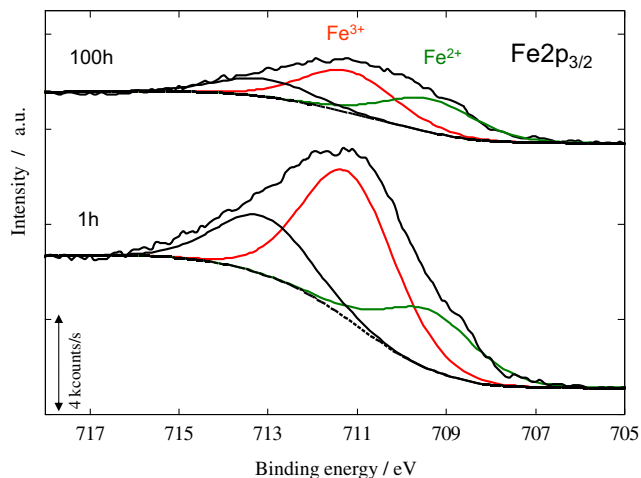


Fig. 2 Fe 2p_{3/2} core level spectra after 1 and 100 h exposure time to high-temperature water

exposure times compared to short exposure times (Table 1). For long exposure time, the intensity ratio between the Ni 2p_{3/2} principal peak and the satellite peak is between 0.3 and 0.7 as for short exposure time. Ni could be associated to Ni(OH)₂ and/or spinel species like (Ni_xFe_{1-x})Cr₂O₄, NiCr₂O₄, or possibly (Ni_{1-y}Fe_y)(Fe_{1-x}Cr_x)₂O₄.

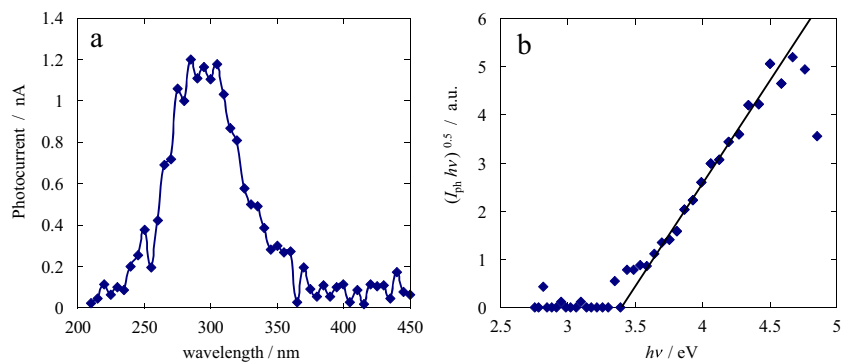
In the early oxidation stage (10 min), a Cr³⁺-rich oxide is formed in the inner part and an Fe³⁺, Fe²⁺-rich oxide in the outer part. The apparent chromium oxide content in Table 1 is low because it was calculated assuming a single mixed oxide and not a multilayer model in which Cr oxide would be in the inner layer (and thus its signal would be attenuated). A significant amount of Ni²⁺ is detected, which may correspond to Ni(OH)₂ and/or a spinel.

For increasing oxidation times (1 and 5 h), the outer oxide layer grows and the signal from the inner chromium oxide layer is attenuated. For longer oxidation times (25 and 100 h), the spinel layer continues to grow at the expense of the outer Fe³⁺ oxide layer, and the signal from Cr³⁺ spinel oxide is less attenuated.

Electrochemical and photoelectrochemical characterisation

We performed a photoelectrochemical investigation in 0.1 M ABE (pH 8.5) at the open circuit potential, U_{OC}, and at slightly higher voltage. We tried to keep the investigated potential range in a narrow interval in order to minimise the changes in film composition due to the anodic polarisation. In Fig. 3, we report the photocurrent spectrum recorded at the open circuit potential, U_{OC} = -0.03 V (Ag/AgCl) for the SS before immersion in high-temperature water, thus relating to the passive film formed by air exposure. Assuming indirect optical

Fig. 3 **a** Raw photocurrent spectrum obtained for the passive film on AISI 316L as supplied recorded by polarising the sample in 0.1 M ammonium baborate at $U_{OC} = -0.03$ V (Ag/AgCl). **b** $(I_{ph}h\nu)^{0.5}$ vs $h\nu$ plot



transitions, it is possible to estimate a band gap value of 3.37 eV according to Eq. (1):

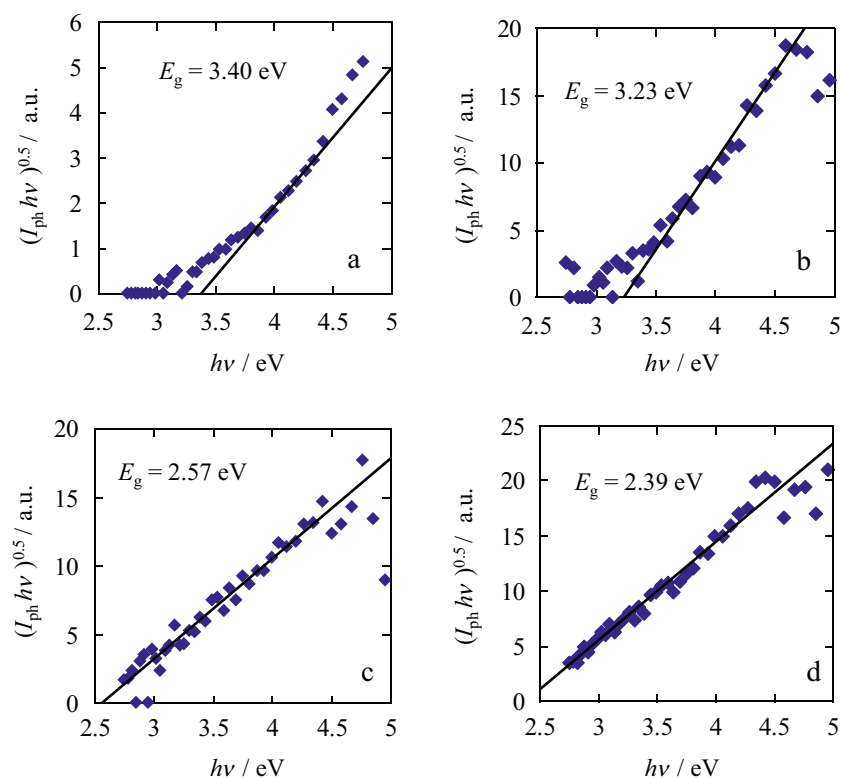
$$(I_{ph}h\nu)^{0.5} \propto (h\nu - E_g) \quad (1)$$

where, for a photon energy in the vicinity of band gap, I_{ph} , the photocurrent is proportional to the light absorption coefficient, $h\nu$ is the photon energy and E_g is the optical band gap.

A very similar U_{OC} was measured for passive films formed by immersion in high-temperature water, but it was not possible to record any photocurrent spectrum due to the very poor photocurrent intensity. However, by moving the polarising voltage toward the anodic direction, we were able to record photocurrent spectra and, thus, to estimate the band gap values of the investigated AISI samples after immersion in high-

temperature water. In Figs. 4 and 5, we report the $(I_{ph}h\nu)^{0.5}$ vs $h\nu$ plots, relating to passive films on as supplied SS and after immersion in high-temperature water, recorded in 0.1 M ABE at 0.3 V (Ag/AgCl), which is a potential slightly higher than the equilibrium potential for chromium oxide dissolution as chromate ions, according to the Pourbaix diagram relating to Cr–H₂O system at room temperature [31]. From the photocurrent spectra, by assuming non-direct optical transitions, it was possible to estimate the band gap of the photoactive phase in the investigated samples. As shown in Fig. 4, after 2 min of immersion in high-temperature water, the band gap of the film is very close to that measured for the stainless steel ($E_g = 3.23$ eV), whilst it decreases to 2.57 and 2.39 eV after 10 min and 1 h of immersion, respectively. For longer immersion times, it is possible to evidence the presence of two linear regions in the $(I_{ph}h\nu)^{0.5}$ vs $h\nu$ plots (see Fig. 5). From the high-

Fig. 4 $(I_{ph}h\nu)^{0.5}$ vs $h\nu$ plots relating to photocurrent spectra recorded for: **a** as supplied SS, **b** after 2 min, **c** 10 min and **d** 1 h of immersion in high-temperature water. Sol: 0.1 M ammonium baborate (pH 8.5) at $U_E = 0.3$ V (Ag/AgCl)



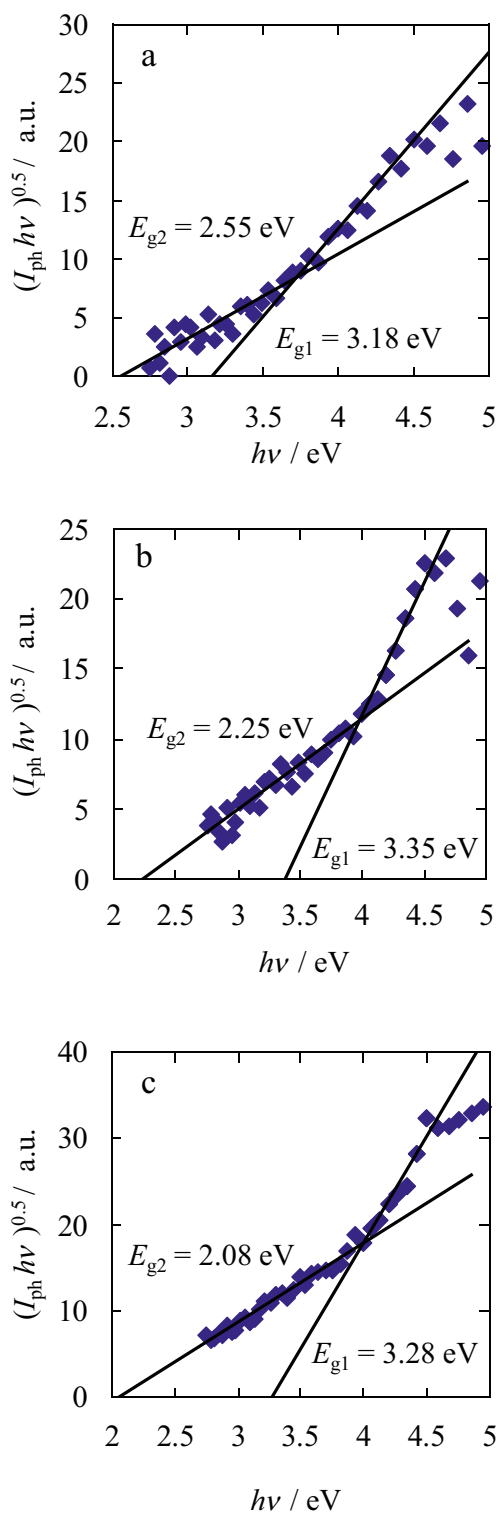


Fig. 5 $(I_{ph}h\nu)^{0.5}$ vs $h\nu$ plots relating to photocurrent spectra recorded for SS after: **a** 5 h, **b** 25 h and **c** 100 h of immersion in high-temperature water. Sol: 0.1 M ammonium baborate (pH 8.5) at $U_E=0.3$ V (Ag/AgCl)

energy region, $E_{g1}=3.25\pm 0.10$ eV can be estimated, whilst a long photocurrent tail is present in the low-energy region, ending at $E_{g2}=2.55$ eV, $E_{g2}=2.25$ eV and $E_{g2}=2.08$ eV for

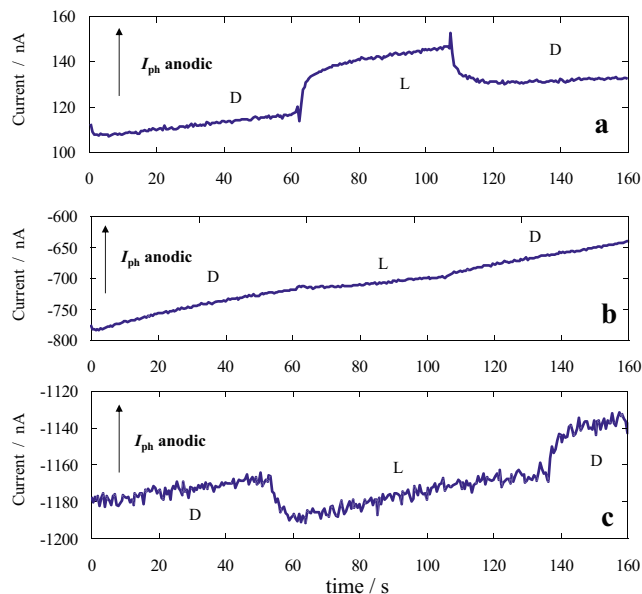


Fig. 6 Current vs time curves recorded at several potentials for SS after 2 min of immersion in high-temperature water: **a** 0.2 V (Ag/AgCl), **b** 0 V (Ag/AgCl), **c** -0.1 V (Ag/AgCl). Sol: 10^{-3} M $FeSO_4$. (pH 5.5). *D* dark and *L* light ($\lambda=300$ nm)

passive films formed after 5, 25 and 100 h of immersion time, respectively.

In order to establish the sign of the measured photocurrent and, thus, the kind of conductivity of the passive films, we recorded current vs time transients under constant wavelength by manually chopping irradiation. In order to increase the ratio between photocurrent and total current, we used an electrolyte containing Fe^{2+} that can be easily photo-oxidised to Fe^{3+} . The

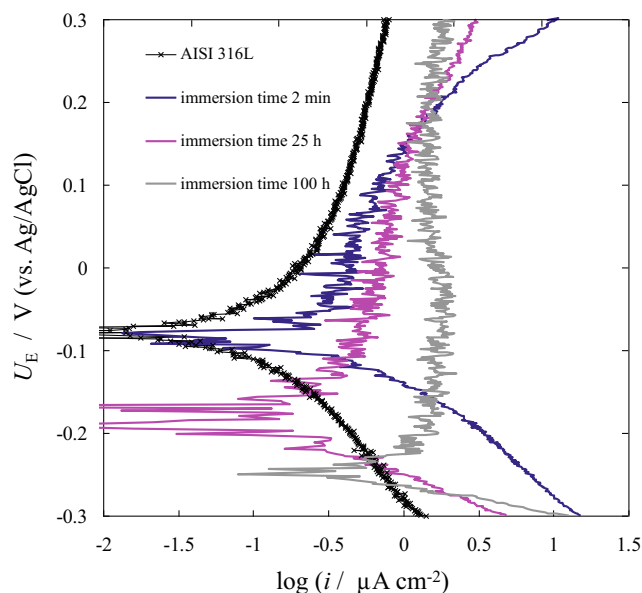
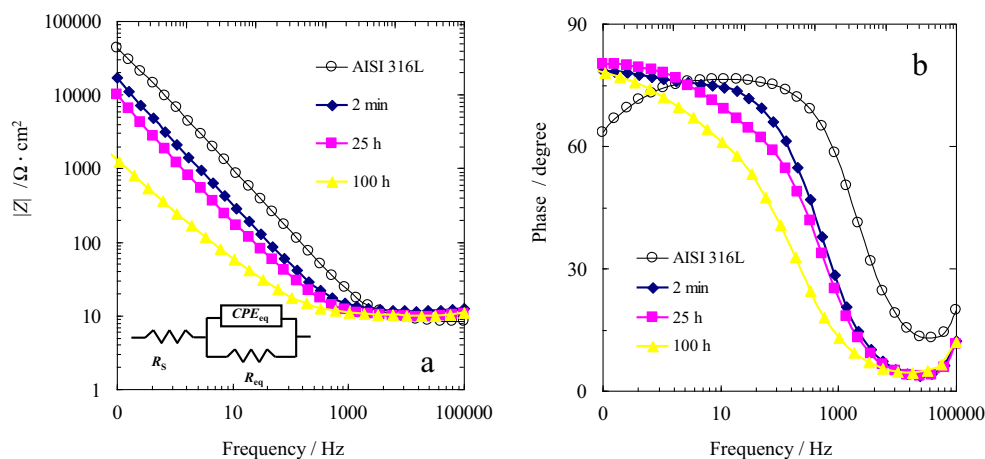


Fig. 7 Polarisation curves relating to passive films on as-supplied AISI 316L and after 2 min, 25 h and 100 h of immersion in high-temperature water, recorded by scanning electrode potential of the sample at 1 mV s^{-1} in 0.25 M Na_2HPO_4 (pH 8.5)

Fig. 8 EIS spectra relating to passive films on as-supplied AISI 316L and after 2 min, 25 h, and 100 h of immersion in high-temperature water, recorded by polarising the samples at 0 V (Ag/AgCl) in 0.25 M Na_2HPO_4 (pH 8.5). **a** Modulus and **b** phase angle. Inset: equivalent circuit



corresponding photo-oxidation process is expected to be thermodynamically favourable and kinetically faster than oxygen evolution reaction, which is the only anodic process occurring in 0.1 M ABE. As shown in Fig. 6 for AISI 316L after 2 min of immersion in high-temperature water recorded at three different potentials in 10^{-3} M FeSO_4 (pH~5.5), the photocurrent changes from anodic to cathodic on going from 0.2 V (Ag/AgCl) to -0.1 V (Ag/AgCl), being almost zero at intermediate potential. This behaviour suggests that the photoactive phase has a flat band potential, U_{FB} , very close to 0 V (Ag/AgCl) at pH 5.5. For longer immersion times in high-temperature water, the photocurrent is anodic at 0 V (Ag/AgCl) and goes to zero at -0.1 V (Ag/AgCl). For such layers, no cathodic photocurrent was measured, as typical of n-type semiconducting material.

Figure 7 shows the polarisation curves for the 316L SS in 0.25 M Na_2HPO_4 solution at 25 °C (pH~8.5). From the polarisation curves, the passive range is determined to be strongly influenced by the immersion time. The corrosion potential shifts toward the cathodic direction the higher is the immersion time. The passivity region ranges from -0.05 to 0.15 V (Ag/AgCl) for short immersion times, whilst it is wider [from -0.25 to at least 0.3 V (Ag/AgCl)] for the steel after 100 h of immersion. At pH 8.5, the equilibrium potential for Cr_2O_3 dissolution as chromate ions, CrO_4^{2-} , is between 0.09 and 0.24 V (Ag/AgCl), depending on the hydration degree of chromium oxide [31]. Thus, it seems that transpassivity occurs due to chromium oxide dissolution for immersion time up to 25 h. However, this oxidation process is not present for film formed after 100 h of immersion in high-temperature water, thus suggesting that the outer layer of this passive film is chromium free.

Based on the polarisation curves, we select to record electrochemical impedance spectra at 0 V (Ag/AgCl), a potential inside the passive region of all the investigated samples. In Fig. 8, we report the EIS spectra in the Bode representation as a function of the immersion time. As a general trend, the dependence of the impedance on the ac signal frequency is

not strongly influenced by the immersion time. A single time constant was observed in the entire potential region investigated. The best fit was obtained for a simple circuit, including the solution resistance in series with a constant phase element $\sim\text{CPE}_{\text{eq}}$ in parallel with a resistance, R_{eq} (see inset of Fig. 8a). Impedance of the constant phase element can be expressed according to the following equation:

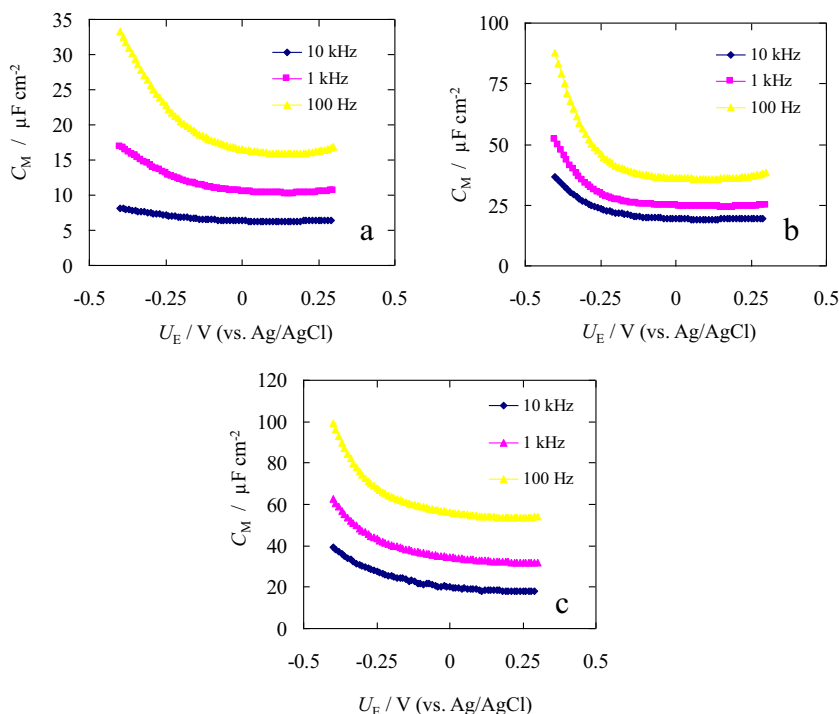
$$Z(\omega) = \frac{1}{(j\omega)^n \text{CPE}} \quad (2)$$

The fitting parameters are reported in Table 2. According to the equivalent circuit of Fig. 8a, the equivalent resistance can be derived as low-frequency asymptote in the modulus vs frequency plot. The Bode plots of Fig. 8 suggest that such equivalent resistance is so high that it cannot be determined accurately in the exploited ac signal frequency range. Moreover, the exponent n of the CPE is <1 , thus suggesting that the constant phase element is simulating a non-ideal capacitor. From Eq. (2), it is possible to estimate the equivalent capacitance, which, for samples before and after immersion in high-temperature water, resulted to be ~ 90 – $150 \mu\text{F cm}^{-2}$, thus significantly higher than the value expected for double layer in aqueous solutions ($C_{\text{H}} \sim 20 \mu\text{F cm}^{-2}$). This poses the problem of understanding its physical meaning, which is also crucial for a correct interpretation of the dependence of the measured capacitance as a function of electrode potential, usually explained in the frame of Mott–Schottky theory (see below).

Table 2 Parameters derived from the best fitting of EIS spectra Fig. 8

Exposure time	R_s ($\Omega \text{ cm}^2$)	R_{eq} ($\Omega \text{ cm}^2$)	Q_{eq} ($\text{S s}^n \text{ cm}^{-2}$)	n
0 min	12.45	$1.9 \cdot 10^4$	$1 \cdot 10^{-4}$	0.75
2 min	11.58	$1.0 \cdot 10^6$	$9.0 \cdot 10^{-5}$	0.85
25 h	9.78	$1.0 \cdot 10^6$	$1.5 \cdot 10^{-4}$	0.83
100 h	10.62	$1.0 \cdot 10^6$	$1.5 \cdot 10^{-4}$	0.83

Fig. 9 Measured series capacitance vs. potential curves recorded in 0.25 M Na₂HPO₄ (pH 8.5), at several frequencies for the passive films on **a** as supplied AISI 316L and after **b** 2 min and **c** 100 h of immersion in high-temperature water



Several authors attributed very high capacitance values measured in the case of passive films on metals to the occurrence of both adsorption phenomena, which introduce a capacitance in parallel with C_H [32–35] as well as to the contribution arising from the surface states, the latter being potential dependent [36]. Moreover, conductive atomic force microscopy allows to evidence a resistance distribution all over the surface samples after immersion in high-temperature water even after short immersion time (i.e., 2 min) [2]. These phenomena make the equivalent circuit necessary to model the metal/passive film/electrolyte interface very complicated, and its validation by a best fitting procedure of the EIS spectra becomes trivial.

In Fig. 9, we compare the measured series capacitance, C_M , vs electrode potential as a function of the frequency of the ac signal for AISI 316L as supplied and after 2 min and 100 h of immersion in high-temperature water. It is clear that the measured capacitance is sensitively influenced by the ac signal frequency, such dependence being not predicted by Mott–Schottky theory [37–39]. Moreover, due the difficulty in the quantitative interpretation of the EIS spectra, and the consequent difficulty in extracting the passive film capacitance from C_M , fitting the curves of Fig. 9 would be misleading.

However, it is important to stress that the capacitance increases by moving the polarising voltage toward the cathodic direction, suggesting that all the passive films behave like n-type semiconducting materials.

The effect of immersion time in high-temperature water on the properties and composition of passive films on SS has been extensively studied in the past [11, 14]. According to a

large number of authors, these films have a multilayered structure with an iron-rich Cr free outer part and Cr-rich inner part. The precise composition of the films is difficult to be determined, due to the very low thickness of the layers and to the difficulty encountered trying to get reliable information from Raman spectroscopy or X ray diffraction [14]. A more sophisticated approach based on local conductivity measurements allowed to further support the formation of a passive film with a Cr-containing inner layer and an outer Fe-rich layer (with Cr oxide of the inner layer being enriched under the grain boundaries of the outer layer) [2].

The photoelectrochemical investigation performed in this work allowed to determine the band gap values of the passive films as a function of the immersion time in high-temperature water. These results, properly matched with the experimental findings provided by XPS, can provide information on structure and composition of the films.

In previous works [40, 41], we suggested and proved that the band gap value of mixed oxides $A_aB_bO_c$ depends on the difference of electronegativity of oxide constituents according to the following relationship:

$$E_g - \Delta E_{am}(\text{eV}) = 1.35(\chi_{av} - \chi_O)^2 - 1.49 \tag{3}$$

Table 3 Electronegativity of major alloying elements of 316L SS

Phase	Cr(III)	Fe(II)	Fe(III)	Ni(II)
$\chi_{Pauling}$	1.60	1.80	1.90	1.80

where χ_{O} is oxygen electronegativity (3.5 in the Pauling scale), and χ_{av} is an average electronegativity parameter, defined as the arithmetic mean between the electronegativities of the metal partners in the oxides, i.e.:

$$\chi_{\text{av}} = \frac{a}{a+b}\chi_{\text{A}} + \frac{b}{a+b}\chi_{\text{B}} \quad (4)$$

$\Delta E_{\text{am}}=0$ for crystalline oxides, whilst increasing values are expected (up to around 0.5 eV) if the lattice disorder affects both density of states distribution near the valence and conduction band edges [42]. Equation (3) allows to get information on the passive film composition as a function of the immersion time in high-temperature water starting from the band gap values. In Table 3, we report the electronegativities of Cr(III), Ni(II), Fe(II) and Fe(III) according to the Pauling scale and the band gap values of their oxides according to the literature [16]. The band gap value estimated for air formed film (see Fig. 3) on as-supplied AISI 316L suggests that such layer is mainly constituted by Cr_2O_3 , as reported in the literature [43]. Moreover, E_{g} is slightly higher with respect to the band gap of crystalline Cr_2O_3 , thus suggesting that the air formed film is amorphous ($\Delta E_{\text{am}} \sim 0.2$ eV) and/or very thin. Due to quantum confinement effect, a blue shift of the optical band gap can be predicted for very thin oxide layers [44]. Anodic polarisation at 0.3 V (Ag/AgCl) does not change significantly the passive film composition, as suggested by the corresponding band gap value (see Fig. 5a). However, it is important to stress that a photocurrent tail in the low-energy region is induced by such polarisation, which suggests that optical transitions at energy lower than E_{g} of Cr_2O_3 occur.

After very short immersion time (i.e., 2 min), $E_{\text{g}}=3.23$ eV, thus slightly lower than that measured for passive film on SS. A significant change in the measured band gap occurs for longer immersion time. More specifically, the band gap decreases, suggesting a change in composition which can be rationalised in the frame of Eq. (3). The measured E_{g} decreases with increasing immersion time from 2 min to 1 h, and if we compare the experimental band gap value with those estimated by Eq. (3) assuming the composition reported in Table 1 for 10 min and 1 h (for which most of the layer thickness is analysed by XPS), we can see that there is a good agreement. However, for longer immersion time, the photoelectrochemical behaviour of passive films changes due the appearance of an appreciable photocurrent tail in the low-energy region of the spectra. This behaviour can be explained assuming the formation of a passive film with a duplex structure constituted by an inner and outer layer with different band gaps, i.e. composition. $E_{\text{g}1}$ values suggest the presence of a Cr rich oxide layer, whilst $E_{\text{g}2}$ estimated from the low-energy region of the photocurrent spectra are compatible with iron rich passive films. Interpretation of the photoelectrochemical results taking into account the

composition estimated by XPS suggests that, during the early stage of immersion (i.e., 2 and 10 min), a chromium-rich passive film is present ($E_{\text{g}}=3.23$ eV), but during immersion in high-temperature water, a $\text{M}(\text{Fe}_{1-x}\text{Cr}_x)_2\text{O}_4$ spinel appears, where M stands for divalent metals (Ni^{2+} and Fe^{2+}). For longer immersion time, the spinel layer continues to grow at the expense of the outer Fe^{3+} oxide layer.

Conclusions

Passive films grown in high-temperature water on AISI 316L were characterised by photoelectrochemical, electrochemical, impedance measurements and X-ray photoelectron spectroscopy.

The photoelectrochemical investigation allowed us to measure a band gap decreasing with increasing immersion time, suggesting a change in the passive film composition. For short immersion time (up to 1 h), the measured photocurrent comes from a Cr-rich oxide layer whose Cr content decreases with increasing immersion time. For longer immersion time (5, 25 and 100 h), we are able to measure photocurrent from a stratified layer with an outer iron-rich layer and an inner Cr-rich oxide layer associated to Cr_2O_3 and $\text{M}(\text{Fe}_{1-x}\text{Cr}_x)_2\text{O}_4$ spinel species, where M stands for divalent metals (Ni^{2+} and Fe^{2+}). For longer immersion time, the spinel layer continues to grow at the expense of the outer Fe^{3+} oxide layer.

According to the current transients recorded under irradiation at constant potential and wavelength, the photocurrent is anodic. This experimental finding and the information arising from the dependence of the measured capacitance on electrode potential suggest that passive films behave as n-type semiconductors, as inverse spinel are expected to be. The presence of cathodic photocurrent for passive films formed after short immersion time (i.e. 2 min) is assigned to electron photoemission processes possible due to the very low thickness of the film.

References

1. Zinkle SJ, Was GS (2013) Acta Mater 61:735–758
2. Massoud T, Maurice V, Klein LH, Seyeux A, Marcus P (2014) Corr Sci 84:198–203
3. Robertson J (1991) Corr Sci 32:443–465
4. Lister DH, Davidson RD, McAlpine E (1987) Corr Sci 27:113–140
5. Stellwag B (1998) Corr Sci 40:337–370
6. Tapping RL, Davidson RD, McAlpine E, Lister DH (1986) Corr Sci 26:563–576
7. Ziemiak SE, Hanson M (2002) Corr Sci 44:2209–2230
8. Terachi T, Fuji K, Arioka K (2005) J Nucl Sci Technol 42:225–232
9. Miyazawa T, Terachi T, Uchida S, Satoh T, Tsukada T, Satoh Y, Wada Y, Hosokawa H (2006) J Nucl Sci Technol 43:884–895
10. Cissé S, Laffont L, Tanguy B, Lafont MC, Andrieu E (2012) Corr Sci 56:209–216

11. Soulas R, Cheynet M, Rauch E, Neisius T, Legras L, Domain C, Brechet Y (2013) *J Mater Sci* 48:2861–2871
12. Gao X, Wu X, Zhang Z, Guan H, Han EH (2007) *J Supercrit Fluids* 42:157–163
13. Sun M, Wu X, Zhang Z, Han EH (2009) *Corr Sci* 51:1069–1072
14. Da Cunha Belo M, Walls M, Hakiki NE, Corset J, Picquenard E, Sagon G, Noel D (1998) *Corr Sci* 40:447–463
15. Szklarska-Smialowska Z, Chou KC, Xia Z (1991) *Corr Sci* 32:609–619
16. Di Quarto F, La Mantia F, Santamaria M (2009) In: Su-II P, Lee JW (eds) *Modern aspects of electrochemistry*, vol 46. Progress in corrosion science and engineering I. Springer, New York
17. Tanuma S, Powell CJ, Penn DR (1994) *Surf Interf Anal* 21:165–176
18. Scofield JH (1976) *J Electron Spectrosc Relat Phenom* 8:129–137
19. Santamaria M, Di Quarto F, Habazaki H (2008) *El Acta* 53:2272–2280
20. Di Quarto F, Santamaria M, Skeldon P, Thompson GE (2003) *El Acta* 48:1143–1156
21. Grimal JM, Marcus P (1992) *Corr Sci* 33:805–814
22. Bussel ME, Marcus P (1992) *Appl Surf Sci* 59:7–21
23. Stypula B, Stoch J (1994) *Corr Sci* 36:2159–2167
24. Atrens A, Lim AS (1990) *Appl Phys A* 51:411–418
25. Clayton CR, Lu YC (1986) *J Electrochem Soc* 133:2465–2473
26. Yamashita T, Hayes P (2008) *Appl Surf Sci* 254:2441–2449
27. Mccafferty E, Bennett MK, Murday JS (1988) *Corr Sci* 28:559–576
28. Ciampi S, Di Castro V (1995) *Surf Sci* 331:294–299
29. Barr TL (1978) *J Phys Chem* 82:1801–1810
30. Machet A, Galtayries A, Zanna S, Klein L, Maurice V, Jolivetn P, Foucault M, Combrade P, Scott P, Marcus P (2004) *El Acta* 49:3957–3964
31. Pourbaix M (1966) *Atlas of electrochemical equilibria in aqueous solutions*. Pergamon Press, Oxford
32. Wikstrom LL, Nobe K (1969) *J Electrochem Soc* 116:525–530
33. Armstrong RD, Bell MF, Metcalfe AA (1977) *J Electroanal Chem* 84:61–72
34. Falkenberg F, Raja VS, Ahlberg E (2001) *J Electrochem Soc* 148: B132–B137
35. Hamnett A (1988) In: Compton RG (ed) *Comprehensive chemical kinetics*, vol 27. Electrode kinetics: reactions. Elsevier, Amsterdam
36. Oskam G, Vanmaekelbergh D, Kelly JJ (1993) *El Acta* 38:301–306
37. Di Quarto F, La Mantia F, Santamaria M (2005) *El Acta* 50:5090–5102
38. Di Quarto F, La Mantia F, Santamaria M (2007) *Corr Sci* 49:186–194
39. La Mantia F, Habazaki H, Santamaria M, Di Quarto F (2010) *Russian J Electrochem* 46:1306–1322
40. Di Quarto F, Sunseri C, Piazza S, Romano MC (1997) *J Phys Chem B* 101:2519–2525
41. Santamaria M, Di Franco F, Di Quarto F, Skeldon P, Thompson GE (2013) *J Phys Chem C* 117:4201–4210
42. Santamaria M, Di Quarto F, Skeldon P, Thompson GE (2006) *J Electrochem Soc* 153:B518–B526
43. Sunseri C, Piazza S, Di Quarto F (1990) *J Electrochem Soc* 137: 2411–2417
44. Beaudoin M, Meunier M, Arsenault CJ (1993) *Phys Rev B* 47: 2197–2202